

COMPRESSIBLE “TURBULENCE” OBSERVED IN THE HELIOSHEATH BY VOYAGER 2

L. F. BURLAGA¹ AND N. F. NESS²

¹ Geospace Physics Laboratory, Code 673, NASA Goddard Space Flight Center, Greenbelt, MD 20771, USA; Leonard.F.Burlaga@NASA.gov

² Institute for Astrophysics and Computational Sciences, Catholic University of America, Washington DC 20064, USA; nfnudel@yahoo.com

Received 2009 June 2; accepted 2009 July 22; published 2009 August 27

ABSTRACT

This paper describes the multiscale structure of the compressible “turbulence” observed in the high-resolution (48 s) observations of the magnetic field strength B made by *Voyager 2* (V2) in the heliosheath behind the termination shock from 2007 DOY 245.0–300.8 and in a unipolar region from 2008 DOY 2.9–75.6. The magnetic field strength is highly variable on scales from 48 s to several hours in both intervals. The distributions of daily averages and 48 s averages of B are lognormal in the post-termination shock (TS) region and Gaussian in the unipolar region, respectively. The amplitudes of the fluctuations were greater in the post-TS region than in the unipolar region, at scales less than several hours. The multiscale structure of the increments of B is described by the q -Gaussian distribution of nonextensive statistical mechanics on all scales from 48 s to 3.4 hr in the unipolar region and from 48 s to 6.8 hr in the post-TS region, respectively. The amplitudes of the fluctuations of increments of B are larger in the post-TS region than in the unipolar region at all scales. The probability density functions of the increments of B are non-Gaussian at all scales in the unipolar region, but they are Gaussian at the largest scales in the post-TS region. Time series of the magnitude and direction of B show that the fluctuations are highly compressive. The small-scale fluctuations are a mixture of coherent structures (semi-deterministic structures) and random structures, which vary significantly from day to day. Several types of coherent structures were identified in both regions.

Key words: circumstellar matter – solar wind – Sun: magnetic fields – turbulence

1. INTRODUCTION

Voyager 1 (V1) crossed the termination shock (TS) on ≈ 2004 DOY 350 (Stone et al. 2005, Gurnett & Kurth, 2005, Decker et al. 2005, Burlaga et al. 2005), and *Voyager 2* (V2) crossed the TS at least five times from 2007 DOY 242–245 (Richardson et al. 2008, Burlaga et al. 2008a, Decker et al. 2008, Gurnett & Kurth, 2008, and Stone et al. 2008). Both spacecraft have been moving through the heliosheath since their crossings of the TS.

V1 observed very large-amplitude fluctuations in the magnetic field strength B at small scales (in the plots of 48 s averages on scales of several hours to tens of days) with very complex profiles (Burlaga et al. 2006a). The fluctuations were described as “turbulence” (Burlaga et al. 2006a, Fisk & Gloeckler 2007), although the nature and origin of these fluctuations are not understood. Since it is not known that there is a cascade of energy associated with these fluctuations and that there is dissipation of energy at very small scales, we cannot claim that the “turbulence” discussed here is analogous to Kolmogorov turbulence. Even if there is an inertial range, the small-scale variations discussed here occur on scales where the proton gyroradius may be important. We shall use the term “turbulence” to denote the small-scale fluctuations observed by V1 and V2 in the heliosheath, without associating a single physical mechanism to all of its manifestations.

The turbulence includes “kinetic-scale” features (with sizes of the order of 10–100 gyroradii), such as isolated magnetic holes and humps, and trains of magnetic holes and humps (Burlaga et al. 2006a). The turbulence also includes “micro-scale” features (> 100 proton gyroradii) that can be described by magnetohydrodynamics (MHD) theory or some variation thereof. It has been argued that the small-scale fluctuations (both kinetic scale and micro-scale fluctuations) are mirror-mode disturbances generated by temperature anisotropies at the termination shock (Liu et al. 2007).

V2 observed complex large-amplitude fluctuations of the 48 s averages of B in the heliosheath. Burlaga et al. (2007b, 2009a) showed that the fluctuations in B observed by V2 behind the TS from 2007 DOY 245–301 (“the post-TS region”) were highly variable during intervals of several hours, with large jumps in B on timescales of minutes to a few hours. They found that the distributions of the increments of B are accurately described by the q -Gaussian (Tsallis) distribution of nonextensive statistical mechanics (Balogna et al. 2000, Moyno et al. 2006, Tsallis 2006a, 2006b, Umarov et al. 2006) on scales from 48 s to 6.8 hr, with $q \approx 1.85 - 1.9$. Large values of q indicate strong intermittency, which is a necessary (but not sufficient) condition for turbulence. Thus, both V1 and V2 observed compressible “turbulence” in the heliosheath. However, the nature of the compressive turbulence and its variability are poorly understood.

The purpose of this paper is to describe the turbulence in a region with a constant magnetic field direction (“the unipolar region”) from 2008 DOY 2–76 and to compare these results with the turbulence observed in the post-TS region discussed by Burlaga et al. (2009a). By means of a comprehensive and quantitative description of the differences of the compressible turbulence in the post-TS region and the unipolar region, we aim to arrive at a better understanding of turbulence in the innermost heliosheath.

On the one hand, the complexity of the observations is so great that one must make use of statistical methods. On the other hand, one cannot understand the structure of the turbulence without appreciating the great variety of time profiles that can be observed in a period of several days or more. Moreover, the heliosheath is inhomogeneous and variable on scales of tens of days or more, as will be illustrated by our comparison of the post-TS region with the unipolar region. We discuss all of these aspects of the turbulence. Section 2 provides an overview of the data, showing the context of the two intervals that will be discussed. Sections 3 and 4 present a statistical description

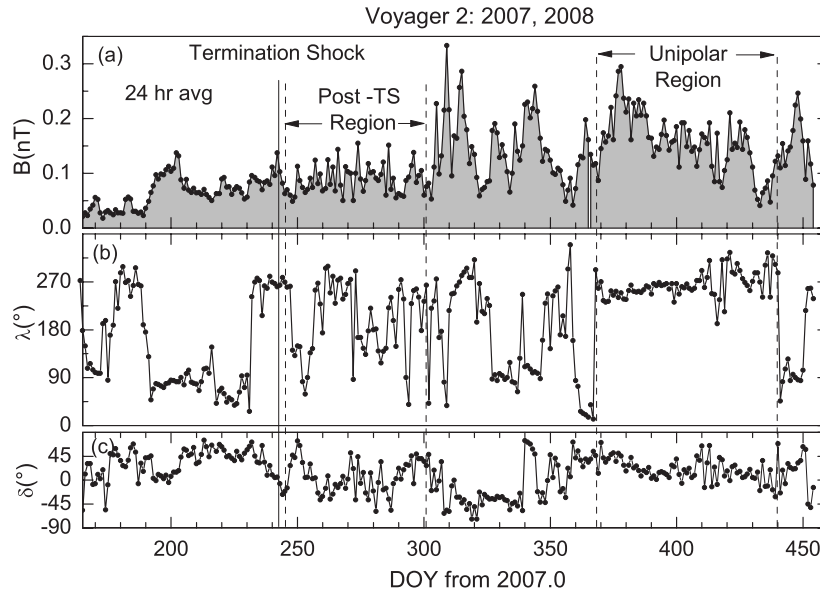


Figure 1. Daily averages of the magnetic field strength B (a) azimuthal angle λ (b) and elevation angle δ (c) from DOY 165 to 453 measured by *Voyager 2* (V2) from the beginning of 2007, showing observations of this supersonic solar wind, the time that V2 crossed the termination shock, and observations of the heliosheath. This paper focuses on the fluctuations of the magnetic field in the post-TS region and the unipolar region identified in this figure.

of fluctuations in B and the increments of B , respectively, on various scales in the post-TS region and the unipolar region, and discuss the differences between the two sets of fluctuations. Detailed time series, illustrating random structures and several types of coherent structures on scales of several hours, are discussed for the two intervals in Section 5.

2. OVERVIEW OF THE VOYAGER 2 MAGNETIC FIELD OBSERVATIONS NEAR THE TERMINATION SHOCK

Since the V2 spacecraft was tracked several hours each day, there are large gaps in the data each day, and on some days there are no data at all. An overview of the observations that we shall discuss is presented in Figures 1(a)–(c), which shows observations of $B(t)$, azimuthal direction $\lambda(t)$, and elevation angle $\delta(t)$, respectively from DOY 165 to 453 measured from DOY 1, 2007. This interval includes both the magnetic field observations made in the solar wind prior to crossing the TS on 2007 DOY 244–245 and observations of the heliosheath behind the TS. Daily averages of B in the solar wind prior to crossing the TS and in the inner heliosheath behind the TS have been discussed by Burlaga et al. (2008b). High-resolution observations (Burlaga et al. 2008a; Richardson et al. 2008) show that the shock strength is ≈ 2 , and that B increased across the TS by that amount. However, no increase in B across the termination shock can be seen in the daily averages of $B(t)$ in Figure 1, because the shock (as seen on small scales) was very dynamic, and it was embedded in a complicated flow.

The profile of $B(t)$ in the heliosheath is highly variable (Figure 1). In the interval from 2007 DOY 245–301 (the post-TS region) B fluctuated about a relatively low value, 0.09 nT, and the magnetic field direction fluctuated in a complicated way. By contrast, in the interval from DOY 367 to 440 B fluctuated about a linear trend, while magnetic field direction was nearly constant at an azimuthal angle ($\lambda \approx 270^\circ$) and an elevation angle elevation angle close to $\delta = 0^\circ$ (the solar equatorial plane). We call this a unipolar region because it is too large to be a sector, given that the speed was $> 100 \text{ km s}^{-1}$ in this region. It is likely that the unipolar region was caused by an excursion of the heliospheric current sheet past the latitude of V2 (Burlaga et al. 2009b).

The distributions of *daily averages* of B in the post-TS region and in the unipolar region are shown in Figures 2(a) and (b), respectively. In the post-TS region, B fluctuates about a nearly constant value ($\langle B \rangle = 0.09 \text{ nT}$), and the distribution of the daily averages of B is lognormal,

$$y = [A/(\sqrt{2\pi}) \times w \times B] \times \exp\{-[\ln(B/B_c)]^2/(2w^2)\}, \quad (1)$$

as shown by the solid curve Figure 2(a), which is a best fit to the data with a coefficient of determination $R^2 = 0.97$. The parameters of the fit are $A = 0.020 \pm 0.001$, $B_c = 0.086 \pm 0.009 \text{ nT}$, and $w = 0.31 \pm 0.02$. The average magnetic field strength is $\langle B \rangle = 0.088 \text{ nT}$ and the standard deviation is $\text{SD} = 0.026 \text{ nT}$.

In the unipolar region, B fluctuates about a linear trend, shown by the line in Figure 2(d). Subtracting the linear trend (“lntrend”) from $B(t)$, we find that the distribution of daily averages of $B' \equiv (B - \text{lntrend})$ is Gaussian

$$y = [A/(\sqrt{\pi/2})w] \times \exp\{-2[(B' - B_c)/w]^2\}, \quad (2)$$

as shown by the solid curve Figure 2(b), which is a best fit to the data with $R^2 = 0.996$. The parameters of the fit are $A = 0.051 \pm 0.002$, $B_c = -0.004 \pm 0.002 \text{ nT}$, and $w = 0.094 \pm 0.003$ (corresponding to $\text{SD} = 0.047 \text{ nT}$). The average magnetic field strength in the unipolar interval is $\langle B \rangle = 0.155 \text{ nT}$, and the standard deviation of the distribution of B is $\text{SD} = 0.054 \text{ nT}$.

The V2 observation of a lognormal distribution of daily observations of B in the post-TS region of the heliosheath was unexpected, because V1 observed Gaussian distributions of daily averages of B in the heliosheath (Burlaga et al. 2006c, 2006d, 2007a, 2008b, 2009c). The distribution of B at large scales in the supersonic solar wind is generally lognormal (Burlaga 2001). It appears that this distribution survived the passage of the solar wind through the TS for at least 57 days, in the post-TS interval. Perhaps this distribution survived because the TS observed by V2 was highly variable and reforming (Burlaga et al. 2008a). This hypothesis suggests further theoretical analysis. Plasma observations by V2 in the heliosheath show cold, supersonic solar wind distributions mixed with the hot heliosheath distributions of protons (Richardson et al. 2008).

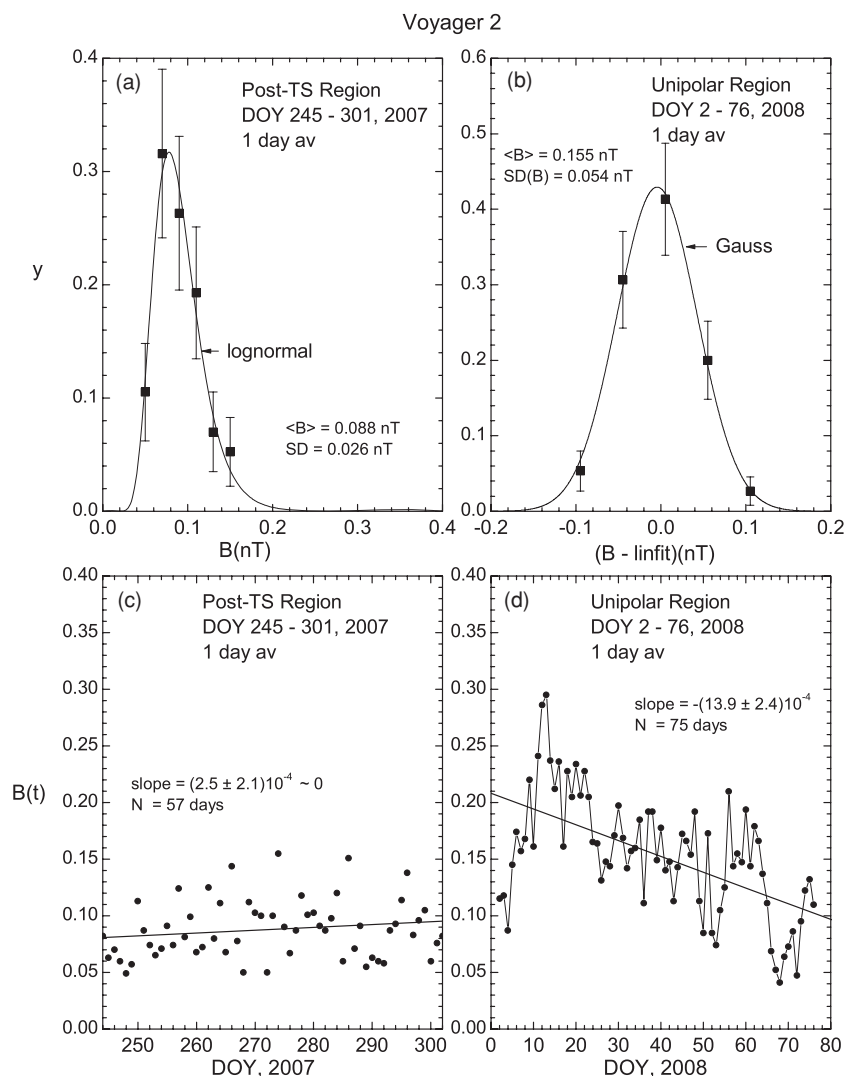


Figure 2. Distributions of daily averages of B in the post-TS region (a) and the detrended daily averages of B in the unipolar region (b), derived from the time series in (c) and (d), respectively.

The plasma in the post-TS region was not fully thermalized, hence not Gaussian.

3. DISTRIBUTIONS OF SMALL-SCALE FLUCTUATIONS OF THE MAGNETIC FIELD STRENGTH

In contrast to the fluctuations of daily averages of B discussed in Section 2 (Figures 1 and 2), we now consider the fluctuations of 48 s averages of B . Plots of the 48 s averages of B versus time observed by V2 in the post-TS region and in the unipolar region are shown as a function of time in Figures 3(a) and (b), respectively. Note that the scale of the ordinate in Figure 3(b) ranges from 0 to 0.4 nT, while the scale of the ordinate in Figure 3(a) ranges from 0 to 0.27 nT. The patterns of the fluctuations in these two intervals are quite different.

In the post-TS interval, the fluctuations of 48 s averages of B tend to be about a constant mean value of ≈ 0.09 nT. A linear fit to the data gives a slope s of only (0.035 ± 0.002) nT/100 day. In the unipolar region, however, the fluctuations are superimposed on a large-scale trend with a mean value of $\langle B \rangle = 0.15$ nT. A linear fit to these data gives a slope of (-0.17 ± 0.001) nT/100 day. In both cases, $\langle B \rangle$ is comparable to the spacecraft magnetic field strength at the outboard sensor

(0.1–0.2 nT), which is highly variable and is the principal source of uncertainty in the measurements. It is important to understand that, even when one considers a plot of high-resolution data such as 48 s averages versus time, the structure of the time series represents fluctuations over a full range of scales from 48 s to the length of the interval under consideration, not just the small-scale structures.

The most significant qualitative features of the fluctuations of $B(t)$ that can be seen in Figure 3 are: (1) the fluctuations can be very large on a scale of several hours; (2) they appear to be larger in the post-TS region than in the unipolar region; and (3) they vary significantly from day to day. In order to quantify the results, we computed the average magnetic strength ($\langle B_i \rangle$), standard deviation $SD(B_i)$ and range(B_i) = ($B_{\max} - B_{\min}$) of the fluctuations of the 48 s averages of B for each day i . Owing to data gaps during each day, the fluctuations described by these statistics are occurring during intervals of ≈ 8 –16 hr.

A measure of the extent of the fluctuations of the 48 s averages of B in the post-TS region and unipolar region is $\langle \text{range}(B_i) / SD(B_i) \rangle = 4.6$ and 4.8, respectively, which is shown in Figure 4. Two measures of the amplitude of the fluctuations, $\text{range}(B_i) / \langle B_i \rangle$ and $SD(B_i) / \langle B_i \rangle$, are plotted in Figure 4. In the post-TS region and the unipolar region, the averages of these

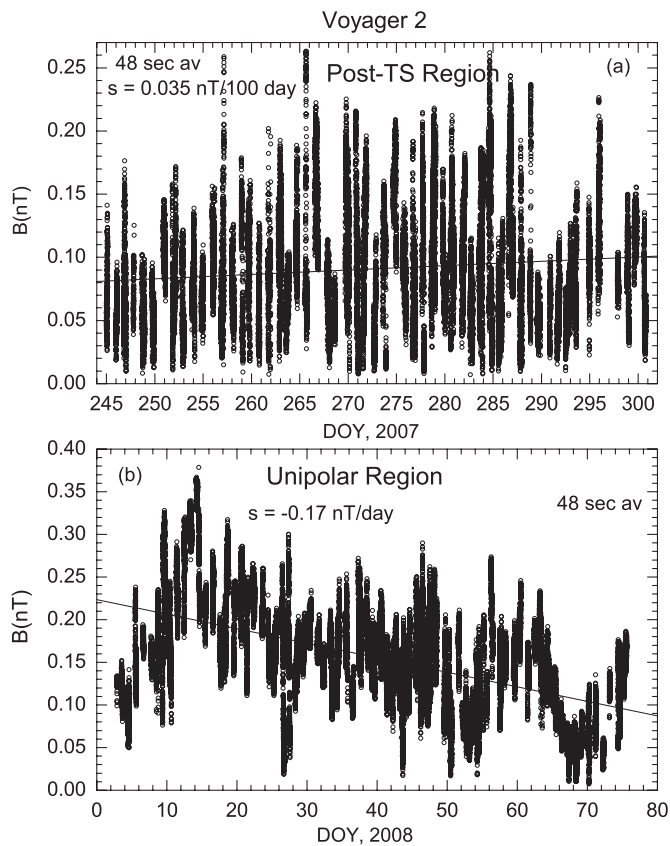


Figure 3. Time series of 48 s averages of $B(t)$ in the post-TS region (a) and the unipolar region (b).

quantities are: (1) $\langle \text{range}(B_i)/\langle B_i \rangle \rangle = 1.63 \pm 0.02$ and 0.81 ± 0.05 , respectively, and (2) $\langle \text{SD}(B_i)/\langle B_i \rangle \rangle = 0.37 \pm 0.02$ and 0.18 ± 0.01 , respectively. These results are shown as lines in Figure 4. Thus, the fluctuations of the 48 s averages of B relative

to the average B on scales less than 1 day in the post-TS region are twice as large as those in the unipolar region.

One expects the fluctuations in the post-TS region to be relatively large. For example, fluctuations of B behind bow shocks of magnetized planets are typically very large compared to the upstream values. Similarly, the fluctuations behind the hydraulic jump produced by water falling from a faucet into a sink (in analogy to the TS) are very large and dynamic. However, it is not known how fast the turbulence generated by the TS decays. Thus, we cannot determine whether the lower turbulence intensity observed in the unipolar region is a result of its larger distance from the TS or a result of a different type of flow moving into the TS.

The values of $\text{range}(B_i)/\langle B_i \rangle$ and $\text{SD}(B_i)/\langle B_i \rangle$ fluctuate from day to day throughout the post-TS region and the unipolar region, as shown by the scatter of the points in Figure 4. The standard deviation $\text{SD}(\text{range}(B_i)/\langle B_i \rangle)$ is 0.48 and 0.42 for all of the days in the post-TS region and the unipolar region, respectively. The corresponding $\text{SD}(\text{SD}(B_i)/\langle B_i \rangle)$ is 0.12 and 0.10 in the post-TS region and the unipolar region, respectively. Thus, the variability of $B/\langle B_i \rangle$ on scales > 1 day is the same in the post-TS region and the unipolar region, respectively.

The distribution of all the 48 s averages of B in the post-TS interval is shown by the points in Figure 5(a). In the post-TS interval, the distribution of the 48 s averages of B is lognormal (the solid curve in Figure 5(a)), within the 95% confidence interval (C.I.). In the unipolar region, a linear fit to $B(t)$ shows a trend, $\text{linfit} = 0.2232 - 0.0017 \times \text{DOY interval}$. The distribution of the 48 s averages of $B' \equiv (B - \text{linfit})$ in the unipolar region is shown by the points in Figure 5(b). In the unipolar region, a fit to the data shows that the distribution of the 48 s averages of B' is Gaussian (the solid curve in Figure 5(b), with $R^2 = 0.99$). The distribution of the 48 s averages of B itself (not shown) is also Gaussian ($R^2 = 0.94$) in the unipolar region. We conclude that the distribution of B in the post-TS region is lognormal, while the distributions of B and B' in the unipolar region are Gaussian.

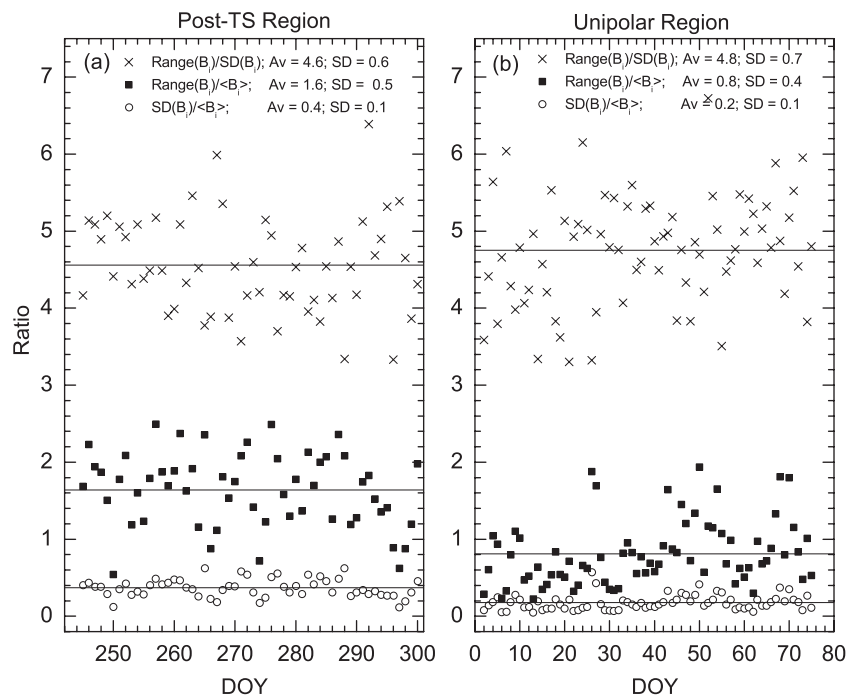


Figure 4. $\text{range}(B_i)/\text{SD}(B_i)$, $\text{range}(B_i)/\langle B_i \rangle$, and $\text{SD}(B_i)/\langle B_i \rangle$ in the post-TS region (a) and unipolar region (b).

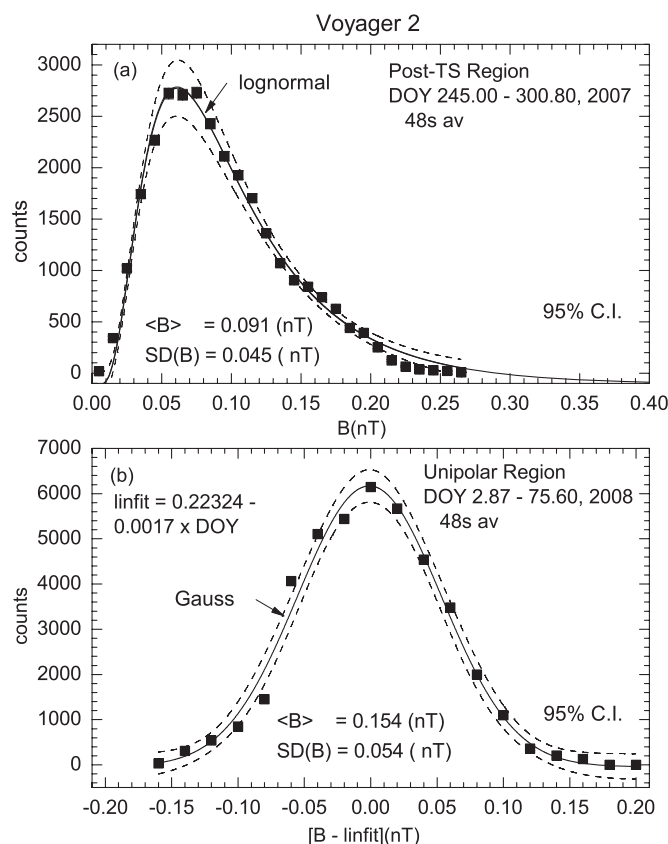


Figure 5. Distribution of 48 s averages of B measured by V2 in the post-TS region (a) and the distribution of detrended 48 s averages of B in the unipolar region (b). The distribution is lognormal in the post-TS region and Gaussian in the unipolar region, as indicated by best-fit curves shown by the solid lines. The dashed curves show the 95% confidence intervals.

In the post-TS region, the distributions of both the daily averages of B and the 48 s averages of B are lognormal. The distribution of daily averages of B (Figure 2(a)) has a smaller standard deviation (0.026 nT) than the distribution of 48 s averages of B (0.045 nT) in the post-TS region. In the unipolar region, the distributions of both daily averages of B (Figure 2(b)) and the 48 s averages of B are Gaussian. The distribution of daily averages of B in the post-TS region has a smaller standard deviation ($SD = 0.035$ nT) than the distribution of 48 s averages of B ($SD = 0.054$ nT) in the unipolar region. The form of the distribution is scale invariant in each region.

The distributions of the daily averages of B are narrower than distributions of 48 s averages of B , because the daily averages of B filter out the small-scale fluctuations. The distribution of daily averages of B describes only the fluctuations on scales >1 day, whereas the distributions of 48 s averages include the contributions of both the small-scale fluctuations and the larger scale fluctuations. Figures 3(a) and (b) and 5 show that the fluctuations of 48 s averages on scales <1 day are very large, comparable to the mean value of B . These small-scale fluctuations make the distributions of 48 s averages broader than the distributions of daily averages, while preserving the form of the distribution functions in the respective regions.

4. DISTRIBUTIONS OF INCREMENTS OF THE MAGNETIC FIELD STRENGTH

The distributions of high-resolution (48 s averages) of $B(t)$ describe the fluctuations of B in the post-TS region and unipolar

region as a whole, but they do not resolve the multiscale structure of the fluctuations. One way to describe the variability of $B(t)$ as a function of scale is to analyze the fluctuations of the increments of B , viz., $dB_m(t) \equiv B(t + \tau_m) - B(t)$ on scales τ_m . This method, which was introduced in early work on velocity fluctuations turbulence in the laboratory (see references in Frisch 1995), has been used to describe turbulent fluctuations of the velocity and magnetic field in the solar wind (for example, Burlaga 1991; Sorriso-Valvo et al. 1999; Marsch & Tu 1994). Burlaga et al. (2003, 2007c) used the distribution of such increments of the daily averages of B to describe magnetic field fluctuations on a large range of scales and distances in the supersonic solar wind, and Burlaga et al. (2009a) used the method to describe small-scale fluctuations in the post-TS region.

This section describes (1) the multiscale increments of B , $dB_m(t)$, in the unipolar region on scales $\tau_m \equiv 2^m \times 48$ s, where $m = 0, 1, 2, 3, \dots, 9$ and (2) the corresponding probability density functions (pdfs) of B on each of these scales. The largest scale that we can consider is determined by the maximum size of the data gaps and the corresponding lengths of the intervals for which we have continuous data. (Although we have continuous observations of daily averages in the post-TS region and the unipolar region, the number of points (days) is too small for a meaningful analysis of distributions of increments of daily averages of B .) This section also compares the results for the unipolar region with those for the post-TS region (which were presented by Burlaga et al. 2009a), showing that the multiscale structure of the fluctuations of B is different in these two regions.

For the unipolar region, Figure 6 shows $dB_m(t)$ on scales $\tau_m \equiv 2^m \times 48$ s for $m = 0, 1, 2, 3, \dots, 9$. The amplitudes of the increments of B increase with increasing scale. There are a few subintervals with relatively large increments in each of the time series; they appear at the same time in all of the time series, but their form varies from one time series to the next. In the time series corresponding to smaller lags, one can see isolated points, some of which appear to be extraneous outliers. These points are very important in determining the tails of the pdfs of the increments of B . Thus, it is necessary to edit the data with extreme care in order to eliminate noise points while retaining the physically significant points in the tails of the pdfs. This is a challenging and labor-intensive process, which cannot be fully automated, thus restricting the size of the data sets, which can be analyzed. At larger scales, there are fewer extreme values and the fluctuations have relatively large amplitudes. The data become increasingly sparse at larger scales, owing to the limited size of contiguous points as a result of the daily data gaps. Overall, Figure 6 shows that the increments of B are highly variable on all scales and are very bursty on the smaller scales, as observed in intermittent turbulence. Qualitatively, the set of profiles of the increments of B have a form similar to that associated with intermittent turbulence.

For the post-TS region, Figure 7 shows $dB_m(t)$ on scales $\tau_m \equiv 2^m \times 48$ s for $m = 0, 1, 2, 3, \dots, 9$. Generally, the forms of these profiles are similar to those in Figure 6 for the unipolar region. However, two significant qualitative differences between the profiles for these two regions are evident. The amplitudes of the fluctuations are generally larger for the post-TS region than for the unipolar region. And large “outliers” are more evident in the temporal profiles for the post-TS region than for the unipolar region. (For example, compare the time series $dB_{2 \times 48s}(t)$ for the two regions.)

The multiscale structure of the increments of B in the unipolar region can be illustrated by plotting a pdf for each time series

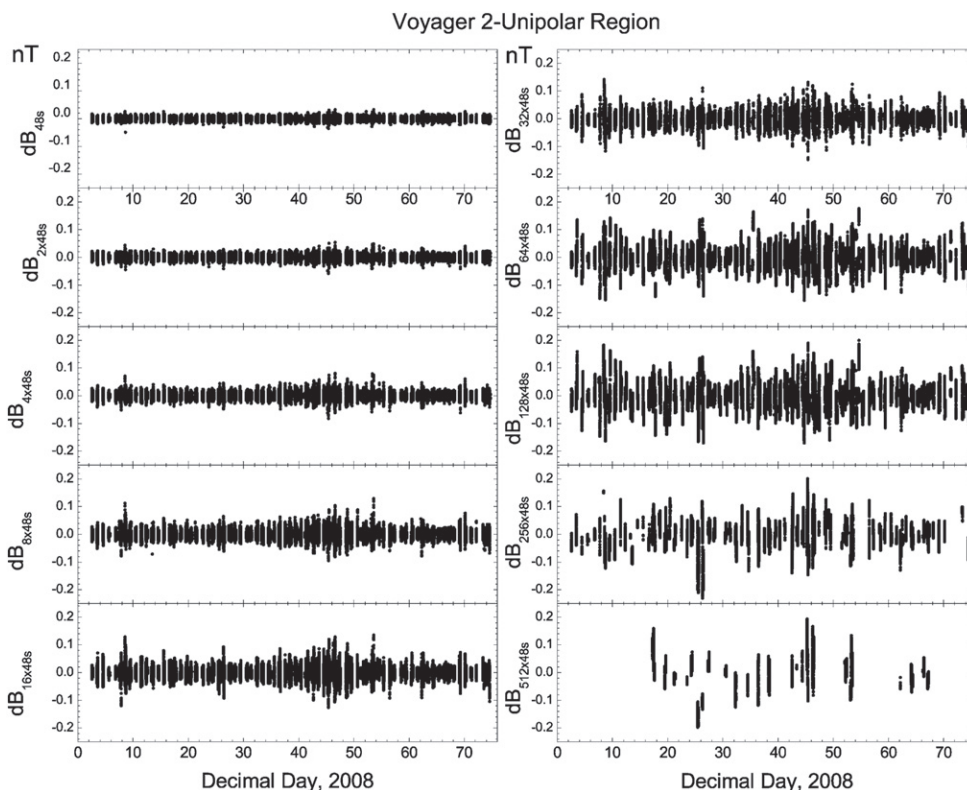


Figure 6. Time series of the increments of B , $dBm(t)$, on scales $\tau = 2^m \times 48$ s, $m = 0, 1, \dots, 8$ based on V2 measurements in the unipolar region.

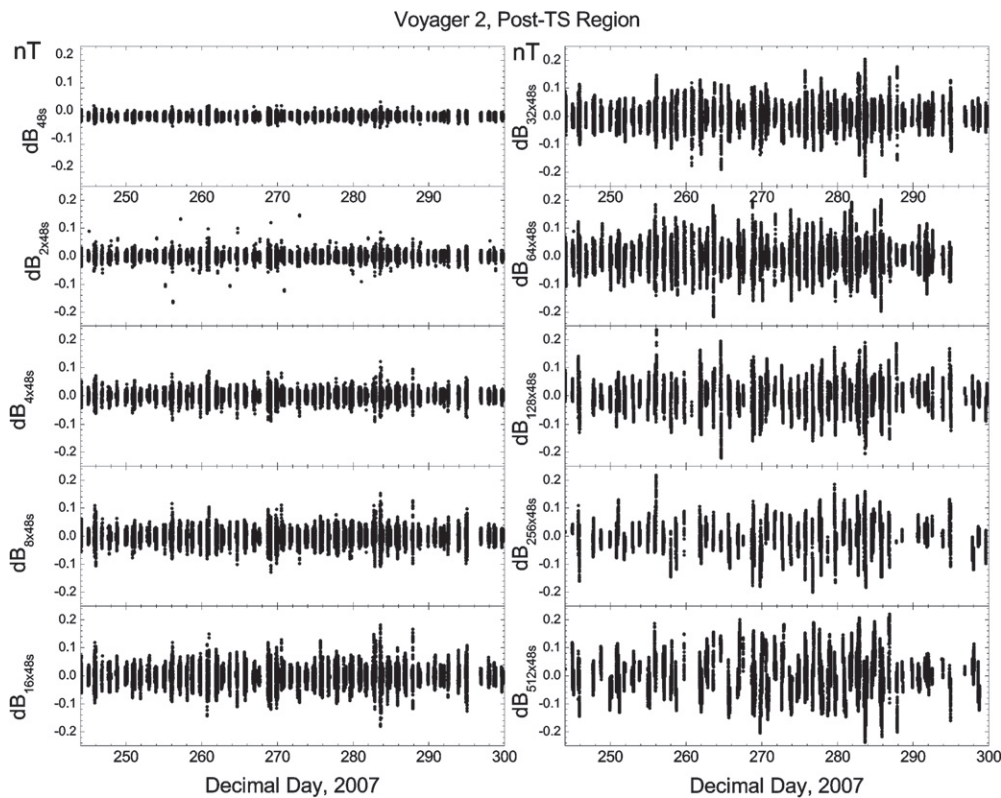


Figure 7. Time series of the increments of B , $dBm(t)$, on scales $\tau = 2^m \times 48$ s, $m = 0, 1, \dots, 9$ based on V2 measurements in the post-TS region.

$dB_{m \times 48s}(t)$. We computed the distribution of increments for each of these time series $dB_{m \times 48s}(t)$, $m = 0, 1, \dots, 8$ normalized by the corresponding total number of points. Each distribution is plotted as a set of points in Figure 8(b), where each pdf is displaced a factor of 100 times above the one below it, for the

sake of clarity. The distributions are labeled by the integer m defined above.

Previous studies have shown that distributions such as these exist over a wide range of distances in the solar wind (Burlaga & Viñas 2004, 2005) and in the heliosheath (Burlaga et al.

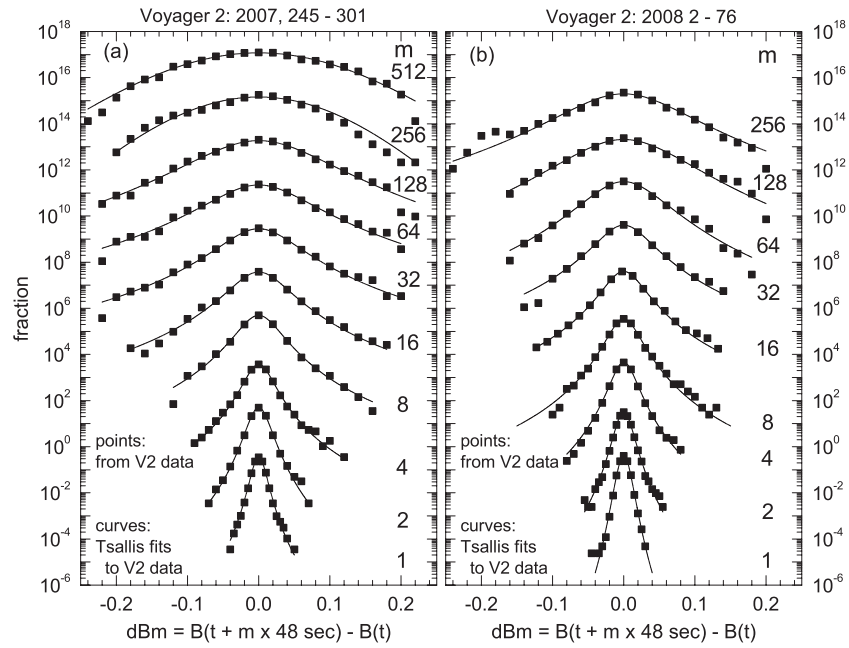


Figure 8. pdfs of increments of B , $dBm(t)$, on scales $\tau = 2^m \times 48$ s, $m = 0, 1, \dots, 9$ for the post-TS interval (a) and $m = 0, 1, \dots, 8$ in the unipolar interval (b). The curves are fits of the observed pdfs to the Tsallis distribution.

2006d, 2007c) on scales greater than or equal to 1 day, and that they can be described by the Tsallis distribution of nonextensive statistical mechanics (Tsallis 1988, 2004), which is related to the q -Gaussian distribution discussed above. Burlaga et al. (2007c) showed that the q -Gaussian distribution describes the pdfs of increments of B predicted by a MHD model for a wide range of scales from 1 to 90 AU in the solar wind, in good agreement with the observations. However, the Tsallis distributions of increments of B in the heliosheath have not been modeled yet.

We fit the distributions of dBm plotted in Figure 8(b) with the q -Gaussian distribution (the symmetric Tsallis distribution), viz.,

$$R_q = A_q [1 + (q-1)\beta_q (dBm)^2]^{-1/(q-1)}. \quad (3)$$

The parameter q (“entropic index” or “nonextensivity parameter”) is related to the size of the tail in the distribution. The parameter $w_q \equiv \beta_q^{-1/2}$ measures the width of the distribution. The coefficients A_q , β_q , and the “entropic index” q are functions of the scale τ_m . A q -Gaussian distribution can describe distributions ranging from Gaussian distributions ($q = 1$) to symmetric distributions with large power-law tails. Intermittency is manifested by the presence of large tails in the distributions of increments of B . The parameter q of the Tsallis distribution provides a measure of the intermittency. The tails are produced by a relatively small number of points, the “outliers” that were referred to in the discussion of Figures 6 and 7.

The fits of Equation (1) to the distributions of dBm observed in the unipolar interval are shown by the solid curves in Figure 8(b) on scales from τ_0 to τ_7 . The fits were obtained using the Levenberg–Marquardt algorithm (Levenberg 1944 and Marquardt 1963) to fit the weighted values of the logarithm of the fraction of counts in the selected bins for dBm . There are 41,303 points in the distributions for 48 s lags ($m = 0$) and 17,700 points in the distributions for $m = 8$. Thus, during the interval under consideration we have data suitable for this analysis for 31.4% and 13.4% of the time at the smallest and largest scales, respectively. The quality of the fits is measured by the coefficient of determination R^2 with values between 0.958

and 0.997. We obtain the important result that the q -Gaussian distribution provides good fits to all of the pdfs of increments of B , on all scales from 48 s to 3.4 hr in the unipolar region.

The pdfs in Figure 8(b) are narrow at small scales and increasingly wider at larger scales. There are conspicuous tails at the smaller scales, corresponding to the “outliers” referred to in the discussion of Figure 6, which are characteristic of intermittent turbulence. Since the pdfs in Figure 8(b) are plotted on a semilog scale, a Gaussian distribution would appear as a parabola. Since a parabola does not provide a good fit for the pdf at any scale, including the largest scale (3.4 hr, corresponding to $m = 8$), the pdfs of increments of B in the unipolar region are non-Gaussian at all scales considered.

For the post-TS region, the pdfs and fits to the q -Gaussian distribution were presented by Burlaga et al. (2009a). They are reproduced in Figure 8(a) for comparison with the pdfs for the unipolar region shown in Figure 8(b). Qualitatively, the widths of the pdfs for the post-TS region are generally larger than those for the unipolar region. Thus, the amplitudes of the fluctuations of increments of B are larger in the post-TS region than in the unipolar region at all scales, consistent with our earlier conclusion based on statistics of B . The tails of the pdfs of the increments of B in the post-TS region at the smaller scales tend to be broader and more kurtotic than the pdfs in the unipolar region. This reflects greater intermittency and more prominent “outliers” in the time series of increments of B for the post-TS region than in the unipolar region.

The tails of the pdfs in Figure 8 are described quantitatively by the entropic index q derived from the fits of the Tsallis distribution to the observations. The parameter q is plotted as a function of scale for the post-TS region and the unipolar region in Figures 9(a) and (b), respectively. The function $q(\tau)$ is narrower for the unipolar region than for the post-TS region, with maximum values at 16×48 s = 768 s and 32×48 s = 1,536 s, respectively. Thus, it might be possible to obtain more reliable estimates of the temperature in the unipolar region than in the post-TS region using the method described by Burlaga et al. (2009a). The maximum values of q in the unipolar region

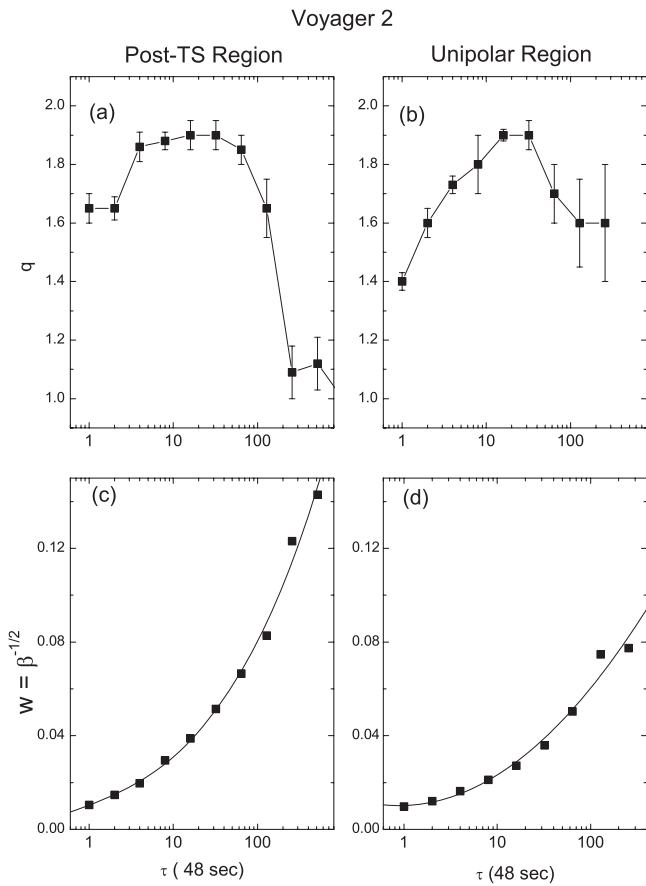


Figure 9. Entropic index q as a function of scale for the post-TS region (a) and the unipolar region (b). The width of the pdfs w as a function of scale for the post-TS region (c) and the unipolar region (d).

are the same as those in the post-TS region, namely $q \approx 1.9$, corresponding to q -Gaussian whose moments do not converge, indicating a relatively strong intermittency.

At the smallest scales in the post-TS region (48 s and 96 s), $q \approx 1.65$, which is close to the value $q \approx 1.75$ that is expected to be relevant for nonlinear systems in which the random variable consists of a sum of strongly correlated contributions, such as dynamical systems at a critical point (Tirnakli et al. 2007). By contrast, at the smallest scales in the unipolar region, $q \approx 1.4$, which corresponds to the observation of fewer “outliers” in the time series $dB_{48s}(t)$ in the unipolar region (Figure 6) than in the post-TS region (Figure 7).

At the largest scales in the post-TS region (Figure 9(a)), $q = 1.1 \pm 0.1 \approx 1$ compared to $q \approx 1.6$ in the unipolar region (Figure 9(b)). This difference expresses the observation that the pdfs of increments of B at the largest scales (3.4 – 6.8 hr) are non-Gaussian in the unipolar region (Figure 9(b)), whereas they are Gaussian ($q = 1$) in the post-TS region (Figure 9(a)).

The widths of the pdfs in Figure 8 are described quantitatively by the parameter w derived from the fits of the Tsallis distribution to the observations. This parameter is plotted as a function of scale for the post-TS region and the unipolar region in Figures 9(c) and (d), respectively. The widths of the pdfs of both the post-TS region and the unipolar region increased non-linearly with scale, as suggested by inspection of the time series of increments of B in Figures 6 and 7, respectively. In fact, the increase of w with scale τ is cubic in the post-TS region and a quadratic in the unipolar region, as shown by the curves in Figure 9(c) and Figure 9(d), respectively. Figures 9(c) and (d)

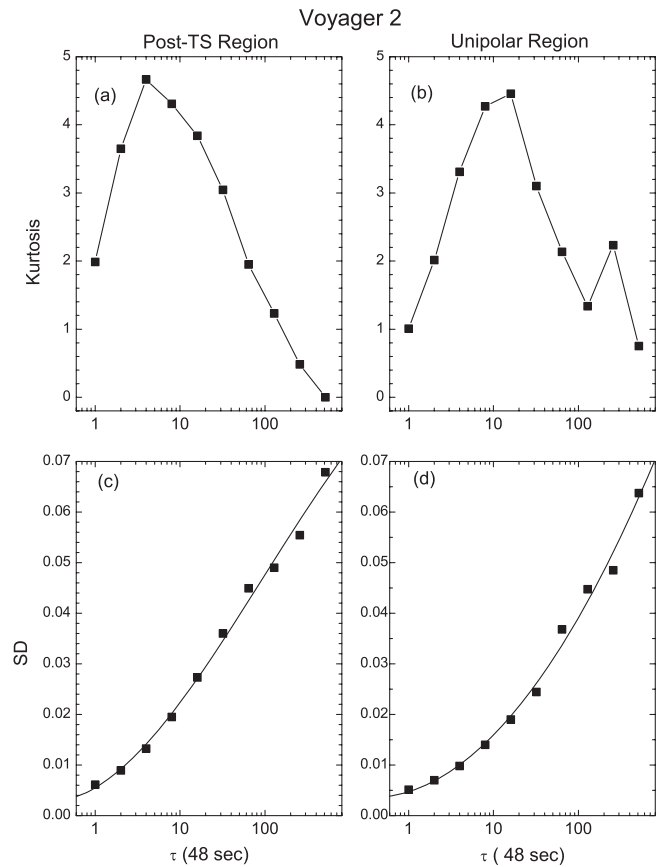


Figure 10. Kurtosis (a) and SD (c) in the post-TS region. The kurtosis (b) and SD (d) in the unipolar region.

show quantitatively that the widths of the pdfs in the post-TS region are larger than those in the unipolar region at all scales. The widths of the pdfs are related to the amplitudes of the fluctuations of the increments of B . In this sense, the turbulence in the post-TS region is more intense than that in the unipolar region.

Previous studies of Tsallis distributions in the solar wind and heliosheath show that the kurtosis and standard deviation of the increments of B are analogous to q and w , respectively. Since K and SD are easier to compute than q and w , it is of interest to examine K and SD as a function of scale for the post-TS region and the unipolar region. Qualitatively, the variations of K and SD with scale τ shown in Figure 10 are similar to those of q and w in Figure 9, but there are some quantitative differences.

5. SMALL-SCALE FLUCTUATIONS

By definition, one can see “small-scale” variations of B in plots of B , λ , and δ versus t on the scale of several hours. In general, the variations differ from day to day. One can identify two classes of fluctuations: (1) “coherent (semi-deterministic) structures” and (2) “random structures” as in gas-dynamic turbulence (Wu et al. 2006). Among the coherent structures, several types of features are observed repeatedly. We classify these features as follows: (1) constant B and constant direction; (2) quasi-periodic B and constant direction; (3) linear magnetic hole; (4) D-sheet; (5) variable B and constant direction; and (6) variable B and variable direction (random structures). The first part of this section illustrates these classes of structures.

An interval in which both the magnitude and direction of B were constant was observed in the unipolar region on 2008 DOY 14 (Figure 11(a)). It might seem remarkable that such uniform

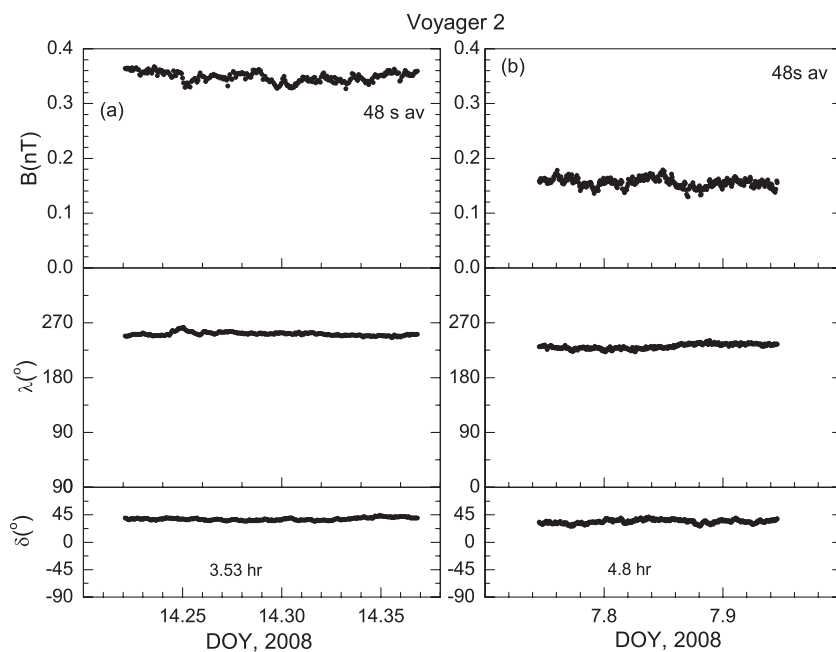


Figure 11. Small-scale structures (a) and (b) with constant magnetic field strength and direction in the unipolar region.

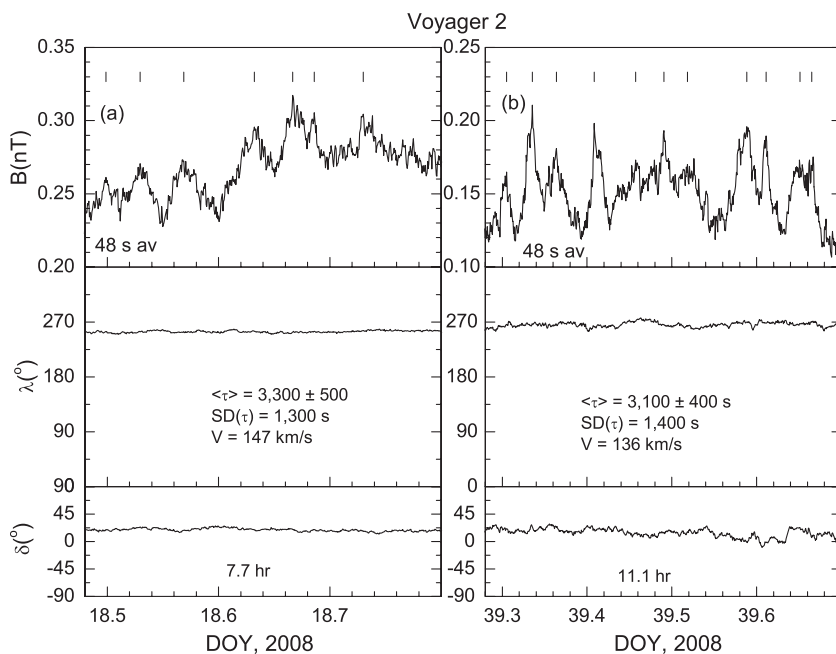


Figure 12. Small-scale structures (a) and (b) with quasi-periodic magnetic field strength and constant direction in the unipolar region.

magnetic fields can be found in the turbulent heliosheath. On the other hand, even in ordinary fluid-dynamic turbulence, intervals of quiescence are observed. One should not assume that the magnetic field is always nonuniform and variable in the turbulent heliosheath on small scales.

Quasi-periodic oscillations in B with very little change in the direction were observed by V2 in the unipolar region on 2008 DOY 18 and 39 (Figures 12(a) and (b)). The short vertical lines at the top of the figures show the times of the local maxima of B . The average interval between the lines is $\langle \tau \rangle = (3300 \pm 500)$ s on DOY 18 and $\langle \tau \rangle = (3100 \pm 400)$ s on DOY 39. The corresponding standard deviations are 1300 s and 1400 s, respectively. Since the speed measured by the plasma instrument on V2 was 147 km s^{-1} and 136 km s^{-1} on 2008 DOY 18 and

39, respectively, the characteristic wavelength of the oscillations was $480,000 \text{ km}$ on DOY 18 and $425,000 \text{ km s}^{-1}$ on DOY 39, respectively. These wavelengths are somewhat larger than the average distance between jumps in B ($153,000 \text{ km}$) observed in parts of the post-TS region discussed by Burlaga et al. (2009a). Given a physical model for the waves in Figure 12, one could perhaps obtain good estimates of the temperature in the heliosheath, using the method presented by Burlaga et al. (2009a).

An observation of a magnetic hole by V2 on 2008 DOY 21 in the unipolar region is shown in Figure 13(a). Magnetic holes were identified in the solar wind at 1 AU by Turner et al. (1977), and they have been found by V1 in the heliosheath both in isolation and in trains (Burlaga et al. 2006a, 2006b), where it

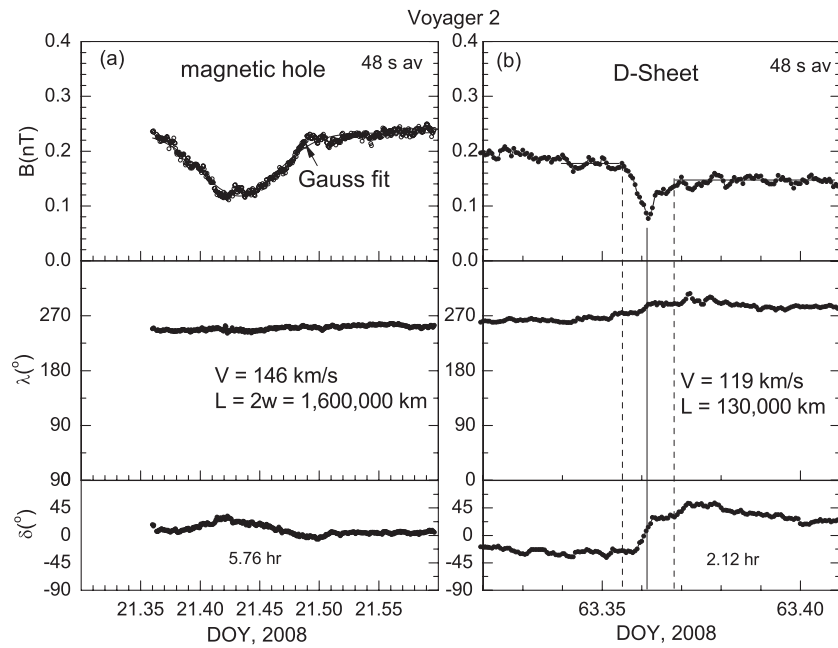


Figure 13. Magnetic hole (a) and the D-sheet (b) in the unipolar region.

was found that the magnetic field strength profile is often nearly Gaussian. The curve in Figure 13(a), a Gaussian fit to $B(t)$ ($R^2 = 0.97$), giving a width $w = 0.065$ nT. Since the speed measured by the plasma instrument on V2 was 146 km s^{-1} , the radial extent of the magnetic hole was $\approx 1,600,000$ km. The physical nature of magnetic holes is not understood, despite the large literature on this subject (see the references in Burlaga et al. (2007b)). Since the direction of \mathbf{B} across the magnetic hole in Figure 13(a) is nearly uniform, this is a “linear magnetic hole” in the terminology of Fitzenreiter & Burlaga (1978). The elevation angle δ appears to be correlated with B in Figure 13(a). However, this apparent correlation is possibly an artifact associated with uncertainties in the measurements. Since the uncertainty of each component of \mathbf{B} is on the order of ± 0.03 nT, the uncertainties in the angles increase when the B decreases, the angles become less well known when $B \approx 0.05$ nT.

An observation of a “D-sheet” by V2 on 2008 DOY 63 in the unipolar region is shown in Figure 13(b). From the speed measured by V2 (119 km s^{-1}), we find that the radial extent of the D-sheet was $30,000$ km. The presence of D-sheets in the heliosheath was demonstrated by Burlaga et al. (2006a) using the *VI* data. The existence of D-sheets, defined as micro-scale depressions in the magnetic field strength associated with discontinuities in the direction of the magnetic field was demonstrated by Burlaga (1968) and Burlaga & Ness (1968). Burlaga & Ness (1968) suggested that D-sheets are a manifestation of magnetic reconnection in the solar wind. Further support for this hypothesis was presented by Burlaga (1968), who discussed a D-sheet in which decrease in B was associated with changes in the speed, density, and temperature, similar to the signature of the magnetic reconnection events recently identified by Gosling et al. (2007) using modern high-resolution data at 1 AU. The available V2 plasma data are not accurate enough to determine the plasma signature of a reconnection event associated with the D-sheet in Figure 13(b), although a peak in the speed is suggestive.

Examples of intervals with variable B and constant magnetic field direction are shown in Figure 14(a) and (b). Note that

B is relatively strong (>0.2 nT) in both of these intervals, so that the angles specifying the magnetic field direction can be determined relatively accurately. The direction of \mathbf{B} is essentially constant in both intervals (2008 DOY 14 and 20 in the unipolar region). On DOY 14, there was a trend of B across the interval and some fluctuations were superimposed on it. On DOY 14, there were two distinct peaks in B superimposed on larger scale fluctuations. A distinctive characteristic of the fluctuations described in Figure 14(b) is that the fluctuations are entirely compressive (no changes in the magnetic field direction).

Finally, we show examples of intervals in the unipolar region in which both the magnitude and direction of the magnetic field are highly variable. These intervals represent random small-scale structures. In this case, B is weak on average. On 2008 DOY 43 (Figure 15(a)), $\langle B \rangle = 0.138$ nT, $SD(B) = 0.045$ nT, the maximum magnetic field strength is $B_{\max} = 0.20$ nT, and the minimum magnetic field strength $B_{\min} = 0.02$ nT. On DOY 54 (Figure 15(b)), $\langle B \rangle = 0.112$ nT, $SD(B) = 0.041$ nT, $B_{\max} = 0.20$ nT, and $B_{\min} = 0.02$ nT. In both cases, B_{\min} is at the level of the uncertainty of the measurements (± 0.03 nT in each component). Measurements of the magnetic field direction have large uncertainties when the magnetic field is this weak. Thus, much of the variability in the direction of the field in Figure 15 may be principally the result of the uncertainties in the measurements. However, detailed analysis of the data shows that some of the variability observed when B is relatively strong might be real, although the angles are not measured accurately. These two examples raise the possibility that the magnetic field direction in the heliosheath is more variable when B is very weak than when it is strong, but it would be, at present, very difficult to prove this, given the uncertainties in the observations.

The few examples of the types of profiles of $B(t)$ observed by V2 that are described above, and the statistical descriptions of all the observations presented in Sections 2 and 3 do not adequately describe the complexity of turbulence in the heliosheath. We conclude this section by showing profiles of $B(t)$ for 20 days in each of the two regions considered in this paper. The reader can best appreciate the complexity by carefully examining these

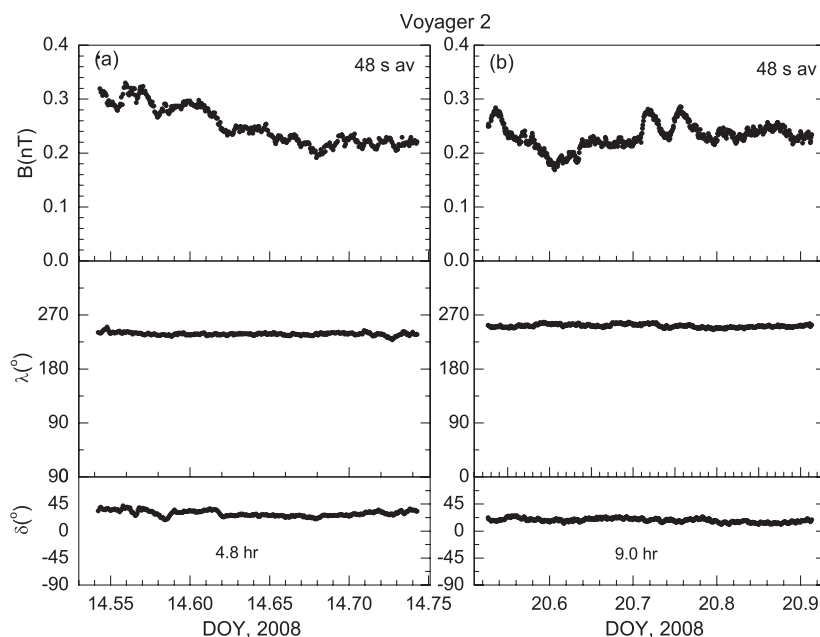


Figure 14. Small-scale structure with variable magnetic field strength and constant direction (a) and (b).

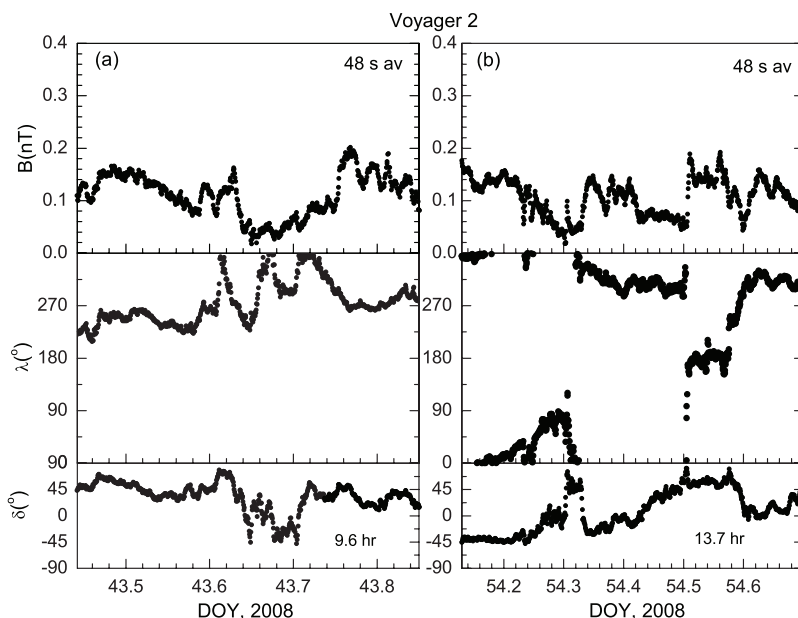


Figure 15. Small-scale structure with variable magnetic field strength and direction (a) and (b). Most of the variability in the magnetic field direction is due to large uncertainties owing to the weak magnetic fields.

profiles. Our intent is to provide the reader a “picture” of the turbulence and a more complete appreciation of its great complexity at small scales.

Figure 16 shows $B(t)$ for several hours in each of 20 consecutive or nearly consecutive days among the 57 days in the post-TS region. This figure shows the broad range of complexity of the variability of B on a scale of several hours. Some of the classes of profiles described above can be seen. The meaning of the statistics presented in Sections 3 and 4 can also be understood by examining the extreme range and rate of variability of B in Figure 16. It is obvious that no simple description of these profiles is adequate. Standard techniques such as power spectrum analysis are, at best, inadequate and, at worst, misleading.

Figure 17 shows $B(t)$ for several hours in each of the 20 consecutive or nearly consecutive days among the 74 days in

the unipolar region. The magnetic field strength is plotted on the same scale (0 – 0.25) nT as the data in Figure 16, but it was necessary to introduce an offset $c \neq 0$ on some days. The comments in the previous paragraph concerning the fluctuations in the post-TS region also apply to the unipolar region shown here. There is no day for which the fluctuations in B can be considered representative of the region. Thus, it will be difficult if not impossible to derive a parameter, such as a diffusion coefficient, that can and will describe propagation of energetic particles in this region.

6. SUMMARY

This paper presents a comprehensive picture of the “turbulence” observed in two regions of the heliosheath by V2.

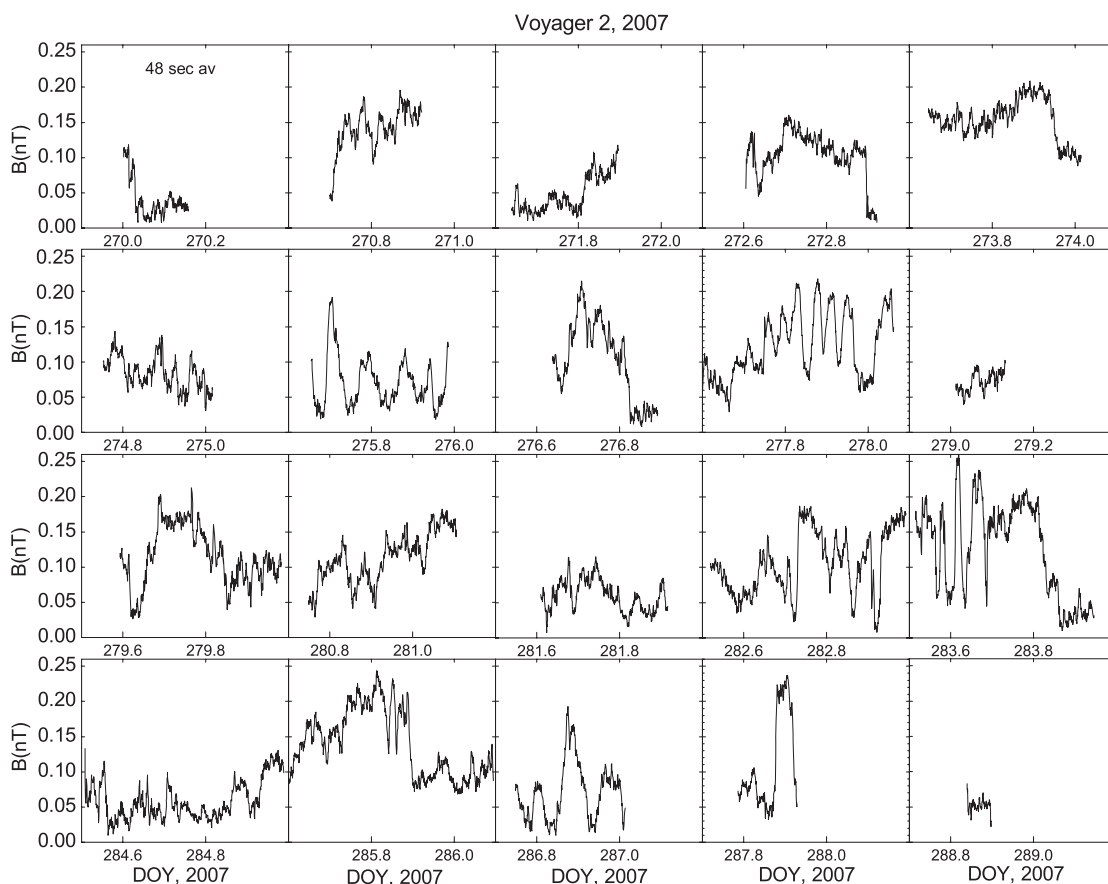


Figure 16. Small-scale structures observed on successive or nearly successive days by V2 in the post-shock region.

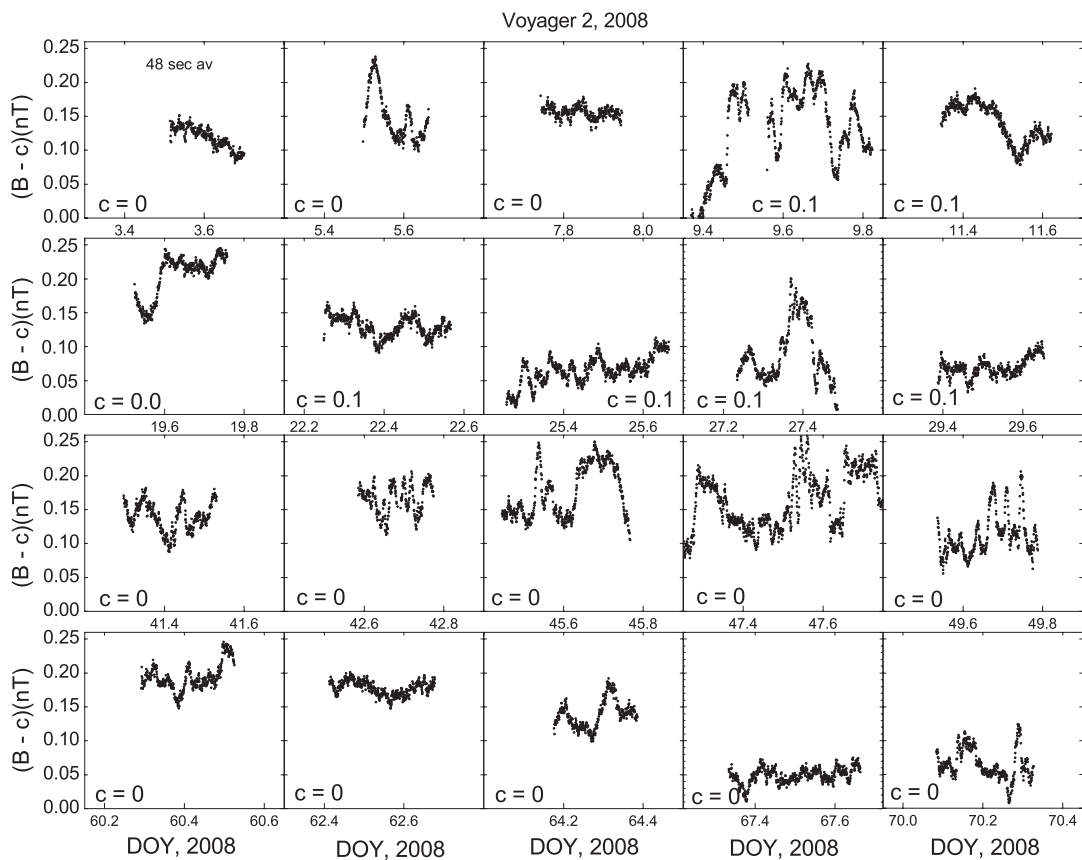


Figure 17. Small-scale structures observed on successive or nearly successive days by V2 in the unipolar region.

We show that turbulence consists of both coherent (semi-deterministic) structures and random structures as seen in time profiles of the magnetic field strength $B(t)$ on scales from 48 s to several hours, which vary greatly from day to day. The paper attempts to provide an appreciation for the complexity and variability of the turbulence. However, it is also shown that, despite the great complexity, there are some simple patterns in the types of coherent structures and the statistical properties of the set of coherent structures and random structures on scales of the order of 60–80 days.

The two regions that were considered are: (1) the “unipolar region” which was observed by V2 in the interval from 2008 DOY 2–76 in which the direction of the magnetic field was nearly constant and (2) the “post-TS region” observed in the interval 2007 DOY 245–301 (just behind the termination shock, TS, which was crossed by V2 at least five times from 2007 DOY 242–245). We show that the fluctuations observed in these two regions differ in some important respects, but share some common properties.

The distributions of daily averages and 48 s averages of the magnetic field strength B are lognormal in the post-TS region and Gaussian in the unipolar region. The lognormal distribution in the post-TS region was not expected, since V1 observed Gaussian distributions everywhere in the heliosheath. It is possible that the lognormal distribution observed that the post-TS region is a remnant of the lognormal distribution that is typically observed in the solar wind. This hypothesis is plausible, because the weak and highly variable TS observed by V2 did not thermalize the solar wind plasma.

The hypothesis that the small-scale turbulence in the heliosheath consists of mirror mode waves that are produced by proton temperature anisotropies generated by a quasi-stationary TS cannot explain (1) the variety of coherent structures and random structures that is observed and (2) the distributions of B and the increments of B . We suggest that in order to understand the turbulence of the heliosheath, it is important to consider the TS that is rapidly evolving on a wide range of scales, including very small scales.

The Gaussian distributions of daily averages and 48 s averages of B observed by V2 in the unipolar region were also observed in the heliosheath by V1. It is possible that the Gaussian distribution in the unipolar region evolved from a lognormal distribution in the post-TS region as the plasma propagated away from the TS. On the other hand, the unipolar region represents a different kind of flow than the post-TS region. The unipolar region might have been produced by different conditions upstream of the TS than the flow in the post-TS region. These hypotheses cannot be tested with the observations, but they should be explored with theories and models.

Since both daily averages and 48 s averages of B in the post-TS region have lognormal distributions, the distribution function is invariant with respect to these scales. Similarly, the observation of a Gaussian distribution of both daily averages and 48 s averages of B in the unipolar region indicates a scale invariance of the distribution in this region as well (as also observed by V1). In both regions, the width of the distribution of daily averages of B was smaller than the width of the distribution of 48 s averages of B . This difference indicates that the fluctuations on scales less than 1 day were significant in both the post-TS region and the unipolar region.

The multiscale structure of the fluctuations was described by studying the increments of B over a range of scales from 48 s to several hours. The time series of increments of $B(t)$ show

highly intermittent fluctuations at smaller scales, associated with coherent (semi-deterministic) structures. These time series are best described quantitatively and statistically by pdfs. It was found that the observed pdfs on scales from 48 s to several hours in both the post-TS region and the unipolar region are described by the symmetric Tsallis distribution of nonequilibrium thermodynamics, which is the same as the q -Gaussian distribution associated with a generalized central limit theorem. In the unipolar region, the pdfs were non-Gaussian at all scales, whereas in the post-TS region the pdfs were Gaussian ($q = 1$) at the largest scales. At the smallest scales, the values of q were in the range expected for turbulence and certain chaotic systems.

Often when one uses a statistical distribution function it is generally assumed that there is one simple underlying stochastic process. However, detailed examination of the time series $B(t)$ observed in the heliosheath during an interval of several hours on each of many days, shows a great variety of profiles, changing significantly from day to day. Various coherent structures are observed in profiles of $B(t)$ during intervals of several hours, including quasi-periodic oscillations with a wavelength $\approx 450,000$ km, magnetic holes, D-sheets, and intervals with no fluctuations in either the magnitude or direction of B . The coherent structures (semi-deterministic structures) are intermingled with random structures in a pattern that changes from day to day. Generally, the fluctuations are compressive in both the post-TS region and the unipolar region. In the unipolar region, there were large changes in B on short timescales but little or no variation in the magnetic field direction.

The variability of the profiles of $B(t)$ is so great within the intervals of several hours and from day to day that it is meaningless to describe it with standard time series methods such as spectral analysis. We suggest it is possible that simple descriptions of transport parameters, such as a constant diffusion coefficient, cannot be derived from the magnetic field observations in the traditional way and are not appropriate for description of the motion of particles of certain energies. Since the Tsallis distribution and q -Gaussian distribution describe the fluctuations of increments of $B(t)$ at all scales between 48 s and several hours in both the post-TS region and unipolar region, we suggest that nonequilibrium statistical mechanics and anomalous transport theory might provide a foundation for statistical descriptions of processes in the heliosheath.

The data in this paper are from the magnetic field experiment on *Voyager 2*. N.F.N. was partially supported by NASA grant NNX07AW09G to the Catholic University of America. McClanahan and S. Kramer carried out the processing of the data. The “0-offset tables” were computed by D. Berdichevsky. The speeds quoted in this paper were derived from the plasma instrument on V2 and provided online by J. Richardson.

REFERENCES

- Balogna, C., Tsallis, C., & Plastino, R. 2000, *Phys. Rev. E.*, **62**, 2213
 Burlaga, L. F. 1968, *Sol. Phys.*, **4**, 67
 Burlaga, L. F. 1991, *Geophys. Res. Lett.*, **18**, 69
 Burlaga, L. F. 2001, *J. Geophys. Res.*, **106**, 15917
 Burlaga, L. F., & Ness, N. F. 1968, *Can. J. Phys.*, **46**, 1962
 Burlaga, L. F., Ness, N. F., & Acuña, M. H. 2006a, *ApJ*, **642**, 584
 Burlaga, L. F., Ness, N. F., & Acuña, M. H. 2006b, *Geophys. Res. Lett.*, **33**, L21106
 Burlaga, L. F., Ness, N., & Acuña, I. H. 2006c, *J. Geophys. Res.*, **111**, A09112
 Burlaga, L. F., Ness, N. F., & Acuña, M. H. 2007a, *ApJ*, **668**, 1246

- Burlaga, L. F., Ness, N. F., & Acuna, M. H. 2007b, *J. Geophys. Res.*, 112, A01106
- Burlaga, L. F., Ness, N. F., & Acuña, M. H. 2009a, *ApJ*, 691, L82
- Burlaga, L., Ness, N. F., Acuña, M. H., Lepping, R. P., Connerney, J. E. P., & Richardson, J. D. 2008a, *Nature*, 454, 75
- Burlaga, L. F., Ness, N. F., Acuña, M. H., Lepping, R. P., Connerney, J. E. P., Stone, E. C., & McDonald, F. B. 2005, *Science*, 309, 2027
- Burlaga, L. F., Ness, N. F., Acuña, M. H., Richardson, J. D., Stone, E., & McDonald, F. B. 2009b, *ApJ*, 692, 1125
- Burlaga, L. F., Ness, N. F., Acuña, M. H., Wang, Y. M., Sheeley, N. R., Wang, C., & Richardson, J. D. 2008b, *J. Geophys. Res.*
- Burlaga, L. F., & Viñas, A. 2004, *J. Geophys. Res.*, 109, A12107
- Burlaga, L., & Viñas, A. 2005, *J. Geophys. Res.*, 110, A07110
- Burlaga, L. F., Viñas, A., Ness, N. F., & Acuña, M. H. 2006d, *ApJ*, 644, L83
- Burlaga, L. F., Viñas, A., & Wang, C. 2007c, *J. Geophys. Res.*, 112, A072106
- Burlaga, L. F., Wang, C., Richardson, J. D., & Ness, N. F. 2003, *ApJ*, 585, 1158
- Burlaga, L. F., et al. 2009c, *J. Geophys. Res.*, 114, A06106
- Decker, R. B., et al. 2005, *Science*, 23, 2020
- Decker, R. B., Krimigis, S. M., Roelof, E. C., Hill, M. E., Armstrong, T. P., Gloeckler, G., Hamilton, D. C., & Lanzerotti, L. J. 2008, *Nature*, 454, 67
- Fisk, L. A., & Gloeckler, G. 2007, *Space Sci. Rev.*, 130, 153
- Fitzenreiter, R. J., & Burlaga, L. F. 1978, *J. Geophys. Res.*, 83, 579
- Frisch, U. 1995, *Turbulence: The Legacy of A.N. Kolmogorov* (Cambridge: Cambridge Univ. Press)
- Gosling, J. T., et al. 2007, *Geophys. Res. Lett.*, 34, L06102
- Gurnett, D. A., & Kurth, W. S. 2005, *Science*, 23, 2025
- Gurnett, D. A., & Kurth, W. S. 2008, *Nature*, 454, 78
- Levenberg, K. 1944, *Q. Appl. Math.*, 2, 164
- Liu, Y., Richardson, J. D., Belcher, J. W., & Kasper, J. C. 2007, *ApJ*, 659, L65
- Marquardt, D. 1963, *SIAM J. Appl. Math.*, 11, 431
- Marsch, E., & Tu, C. Y. 1994, *Ann. Geophys.*, 12, 1127
- Moyno, C., Tsallis, A., & Gell-Mann, M. 2006, *Europhys. Lett.*, 73, 813
- Richardson, J. D., Kasper, J. C., Wang, C., Belcher, J. W., & Lazarus, A. J. 2008, *Nature*, 454, 63
- Sorriso-Valvo, L., Carbone, V., Veltri, P., Consolino, G., & Bruno, R. 1999, *Geophys. Res. Lett.*, 26, 1801
- Stone, E. C., Cummings, A. C., McDonald, F. B., Heikkila, B. C., Lal, N., & Webber, W. R. 2005, *Science*, 23, 2017
- Stone, E. C., Cummings, A. C., McDonald, F. B., Heikkila, B. C., Lal, N., & Webber, W. R. 2008, *Nature*, 454, 71
- Tirnakli, U., Beck, C., & Tsallis, C. 2007, *Phys. Rev. E*, 75, 040106-1
- Tsallis, C. 1988, *J. Stat. Phys.*, 52, 479
- Tsallis, C. 2004, in *Nonextensive Entropy-Interdisciplinary Applications*, ed. M. Gell-Mann & C. Tsallis (New York: Oxford Univ. Press), 1
- Tsallis, C. 2006a, *Milan J. Math.*, 3, 145
- Tsallis, C. 2006b, *Progr. Theor. Phys. Suppl.*, 162, 1
- Turner, J. M., Burlaga, L. F., Ness, N. F., & Lemaire, J. F. 1977, *J. Geophys. Res.*, 82, 1921
- Umarov, S., Steinberg, S., & Tsallis, C. 2006, arXiv:cond-mat/0603593
- Wu, J.-Z., et al. 2006, *Vorticity and Vortex Dynamics* (Berlin: Springer)